CMS Physics Analysis Summary

Contact: cms-pag-conveners-smp@cern.ch 2016/06/24

Measurements of ϕ^* differential cross sections for Drell–Yan events in pp collisions at $\sqrt{s} = 8$ TeV

The CMS Collaboration

Abstract

Measurements of ϕ^* differential cross sections for inclusive Drell–Yan events in the dielectron and dimuon final states are presented. The kinematic variable ϕ^*, constructed from the lepton angles, is correlated with the transverse momentum of the vector boson. The data were collected with the CMS experiment at a centre-of-mass energy of 8 TeV and correspond to an integrated luminosity of 19.7 fb^{-1}. The differential cross section $\mathrm{d}\sigma/\mathrm{d}\phi^*$ normalised to the total cross section within the fiducial volume is measured with a precision of about 1% and is compared with theoretical predictions. The measured spectrum, for the range $\phi^* < 0.1$, differs from the theoretical predictions by at most 5% (ResBos), 4% (MADGRAPH) and 9% (POWHEG). For higher values of ϕ^* the deviations are as high as 9%, 5% and 18% in the three cases respectively.

1 Introduction

The neutral current Drell–Yan (DY) process, $q\bar{q} \to \mathrm{Z}/\gamma^* \to \ell^+\ell^-$, where ℓ is either an electron (e) or a muon (μ), is one of the best-studied benchmark physics processes at the LHC. The total cross sections have been measured at several center-of-mass energies and compared to calculations carried out in perturbation theory at next-to-next-to-leading-order (NNLO) in strong coupling constant α_s [1, 2]. Recently the fully differential NNLO calculation has been matched with higher-order resummation in the 0-jettiness resolution variable [3] which underlines the importance of the process and hence the motivation for studying it using state-of-the-art techniques. The differential cross section $\mathrm{d}\sigma/\mathrm{d}M$ has been measured as a function of the dilepton invariant mass, M [4–7], and theoretical calculations [8] reproduce the data at the few percent level over nine orders of magnitude. The large production cross section and the experimentally clean final state allows for detailed studies of the kinematic distributions for the DY process and these serve as excellent tests of perturbative calculations. The distribution of the transverse momentum q_T of the Z boson is one of the most interesting among these. Relatively low values of q_T are caused by multiple soft gluon emissions, while high q_T values result from the emission of one or more hard partons in the initial state. The differential cross sections $\mathrm{d}\sigma/\mathrm{d}q_T$ have been measured by ATLAS and LHCb at 7 TeV [9, 10] and by CMS at both 7 TeV and 8 TeV [11, 12]. Calculations based on fixed-order perturbation theory [13] describe these measurements fairly well. Recently CMS has extended the study by double-differential measurements in bins of q_T and pseudorapidity [14].

A thorough understanding of the transverse momentum spectra of the vector bosons at hadron colliders is essential for a future high precision measurement of the mass of the W boson. Furthermore, the theoretical calculation of the transverse momentum distribution for Higgs bosons produced in gluon-gluon fusion involve Sudakov form factors that are related to those that appear in the calculations for vector bosons, so measurements of vector boson production at low q_T are important for validating theoretical calculations of Higgs boson production.

A central issue in the measurement of $\mathrm{d}\sigma/\mathrm{d}q_T$ is the experimental resolution of q_T, which is dominated by the uncertainty on the magnitudes of the lepton transverse momenta. The lepton angles, however, are relatively well measured. A new kinematic quantity has been recently introduced [15–17] that is a function of the lepton angles only. It is defined as,

$$\phi^* = \tan\left(\frac{\phi_{\mathrm{acop}}}{2}\right)\sin(\theta^*_\eta)$$

where $\phi_{\mathrm{acop}} \equiv \pi - \Delta\phi$, $\Delta\phi$ being the opening angle between the leptons in the plane transverse to the beam axis. The angle θ^*_η indicates the scattering angle of the leptons in the rest frame of the dilepton system with respect to the beam axis. The angle θ^*_η can be defined in terms of the pseudorapidities of the two oppositely charged leptons as: $\cos(\theta^*_\eta) = \tanh[(\eta_- - \eta_+)/2]$. By construction, $\phi^* \geq 0$. For a dilepton mass in the vicinity of the nominal Z boson mass, ϕ^* correlates well with q_T, and the range $\phi^* \leq 1$ corresponds to q_T up to about 100 GeV. Since ϕ^* depends on angular variables only, the resolution of ϕ^* is significantly better than the resolution of q_T, especially at low q_T.

The ϕ^* distributions for the DY process have been measured by the D0 Collaboration at the Tevatron for $\mathrm{p\bar{p}}$ collisions at $\sqrt{s} = 1.96$ TeV [18] and at the LHC by the ATLAS Collaboration for pp collisions at $\sqrt{s} = 7$ TeV [19]. We present the first measurement of the differential cross section $\mathrm{d}\sigma/\mathrm{d}\phi^*$ using di-lepton events produced in pp collisions at $\sqrt{s} = 8$ TeV, for data collected by CMS experiment corresponding to an integrated luminosity $\mathcal{L} = 19.7 \pm 0.5$ fb^{-1}.

2 Event Selection

The events are selected online using single lepton triggers during the 2012 pp collision data taking period. Due to high instantaneous luminosity, there are multiple soft collisions during the same bunch crossing, as well as crossings just before and after, leading to event pileup (PU) in the detector. The average number of PU events per beam crossing is 21.

Electrons and muons are reconstructed and calibrated using the Particle Flow algorithm [20, 21]. Electron candidates are reconstructed as a charged track in the Tracker pointing to a cluster of energy deposit in the ECAL [22]. Muon candidates are identified as charged tracks in the Tracker that are compatible with charged-particle tracks in the muon system [23]. Quality criteria are applied to the lepton candidates. Events with two leptons are selected in which one lepton, consistent with the trigger, satisfies $p_{\mathrm{T}} > 30$ GeV and $|\eta| < 2.1$, while the other lepton has $p_{\mathrm{T}} > 20$ GeV and $|\eta| < 2.4$. The leptons must have the same flavor and originate from the same primary vertex, defined as the vertex in the event with the largest $\sum p_{\mathrm{T}}^2$, where the sum runs over all tracks associated with the vertex. For dimuon events, the muons must have opposite electric charge. Events are retained if the dilepton invariant mass falls in the range $60 < M_{\ell\ell} < 120$ GeV.

The leptons produced in the DY process are usually isolated from other activity in the event, so isolation criteria are applied to reject non-DY events. The isolation of a lepton is calculated relative to its transverse momentum by summing the transverse momenta of charged hadrons, neutral hadrons, and photons that fall within a cone of radius $\Delta R = \sqrt{\Delta\eta^2 + \Delta\phi^2}$. The values optimized for electrons and muons are $\Delta R < 0.3$ and $\Delta R < 0.4$, respectively. The requirement that the reconstructed tracks originate from a common primary vertex eliminates the pileup contribution to charged hadrons, but the pileup contributions for neutral hadrons and photons must be estimated on a statistical basis. The specific formulae are:

$$I^{e}_{\mathrm{PF}} = \left(\sum p_{\mathrm{T}}^{\mathrm{charged}} + \mathrm{MAX}\left[0, \sum p_{\mathrm{T}}^{\mathrm{neutral}} + \sum p_{\mathrm{T}}^{\gamma} - \rho \times A_{\mathrm{eff}}\right]\right) / p_{\mathrm{T}}^{\mathrm{e}},$$
$$I^{\mu}_{\mathrm{PF}} = \left(\sum p_{\mathrm{T}}^{\mathrm{charged}} + \mathrm{MAX}\left[0, \sum p_{\mathrm{T}}^{\mathrm{neutral}} + \sum p_{\mathrm{T}}^{\gamma} - 0.5 \sum p_{\mathrm{T}}^{\mathrm{PU}}\right]\right) / p_{\mathrm{T}}^{\mu}$$

where ρ is the average transverse energy per unit area and A_{eff} is a parameter tuned to give the best electron purity. Here $0.5 \sum p_{\mathrm{T}}^{\mathrm{PU}}$ refers to the contribution by the neutral particles lying within the isolation cone but not associated with the primary vertex, assuming the contribution to be half of the charged track contribution. The threshold for isolation for electron is $I^{e}_{\mathrm{PF}} < 0.15$, while for muon it is $I^{\mu}_{\mathrm{PF}} < 0.12$.

The efficiencies for the trigger, reconstruction, identification and isolation requirements are obtained in bins of p_{T} and η using tag-and-probe techniques [23, 24]. Correction factors are applied that scale the efficiencies obtained from the simulation to those obtained from the collision data.

3 Simulated event samples

Simulated samples have been used for the determination of the acceptance and efficiencies of the signal as well as for estimating some of the background rates. Large signal samples were generated at next-to-leading order accuracy using the POWHEG generator [25–28] with the CT10NLO parton distribution function (PDF) [29]. For POWHEG the renormalization and factorization scales are determined by the value of the variable $\sqrt{M_{\mathrm{Z}}^2 + q_T^2}$. Parton shower and the hadronization effects are introduced by interfacing with PYTHIA (v. 6.422) [30] using

the Z2star tune [31] determined by studying a sample of minimum bias events analysed by the CMS experiment at $\sqrt{s} = 7\,\text{TeV}$ [32]. An alternative signal sample corresponding to inclusive DY production with up to four hard jets was produced with the MADGRAPH leading-order matrix-element generator [33] using the CTEQ6L1 PDF [34] and interfaced with PYTHIA (v. 6.422).

The backgrounds from $\mathrm{t\bar{t}}$ production, DY$\rightarrow \tau\tau$ and W+jets events were generated using MADGRAPH. Di-boson (WW, WZ and ZZ), the single-top (tW and $\bar{\mathrm{t}}$W), and the muon-enriched QCD multijet samples were generated using PYTHIA. The cross sections for the simulated processes are normalized with the best available theoretical calculations. For the signal and W+jets samples, the total cross sections have been normalized to the value obtained from the NNLO theoretical prediction, given by FEWZ [8]. The $\mathrm{t\bar{t}}$ rate is normalised to the NNLO + next-to-next-to-leading logarithm (NNLL) predicted cross section from Ref. [35]. The single top-quark and diboson cross sections have been calculated at NLO accuracy while the rate for QCD multijets is available only at leading order (LO). The generated events are passed through a CMS detector simulation based on the GEANT4 [36] package.

Minimum bias events have been superposed on the events in all of the above simulated samples to account for pileup. The number of superposed PU events follows the measured distributions, which are a function of instantaneous luminosity.

Scale factors are applied to the simulated samples to account for the differences in the efficiencies measured with data and simulation. The scale factors for electron trigger, identification and isolation efficiencies depend on the ranges of pseudorapidity and transverse momentum. The values range from 0.982 to 1.005 with an uncertainty of 0.1 to 1.2%. For the muon channel the scale factor for the trigger efficiency varies from 0.97 to 1.01, depending on the transverse momentum and pseudorapidity of the muon, with a typical uncertainty of 0.2%. For the identification and isolation efficiencies the combined scale factor ranges from 0.92 to 1.03 with an uncertainty of about 0.5% per muon. Energy/momentum scale corrections are applied to the leptons in both data and simulated events.

Applying the full set of selection criteria, the dielectron and dimuon data sample include about 4.5 million and 6.7 million events respectively. The q_T spectra in the electron and muon channels are presented in Fig. 1. The signal Monte Carlo samples are those generated with POWHEG. The error bars reflect only the statistical uncertainties from the data and the simulated events. While the data include the effects of multiple partons produced in the final state, the POWHEG sample is generated for only zero or one final-state parton. Consequently, the observed q_T spectrum should be harder than that from POWHEG, and discrepancy visible in Fig. 1 is expected.

The ϕ^* distribution is presented in Fig. 2 in 34 bins of varying width. The prediction based on POWHEG singals and background processes are also shown. The bulk of the events lie in the range $\phi^* < 1$.

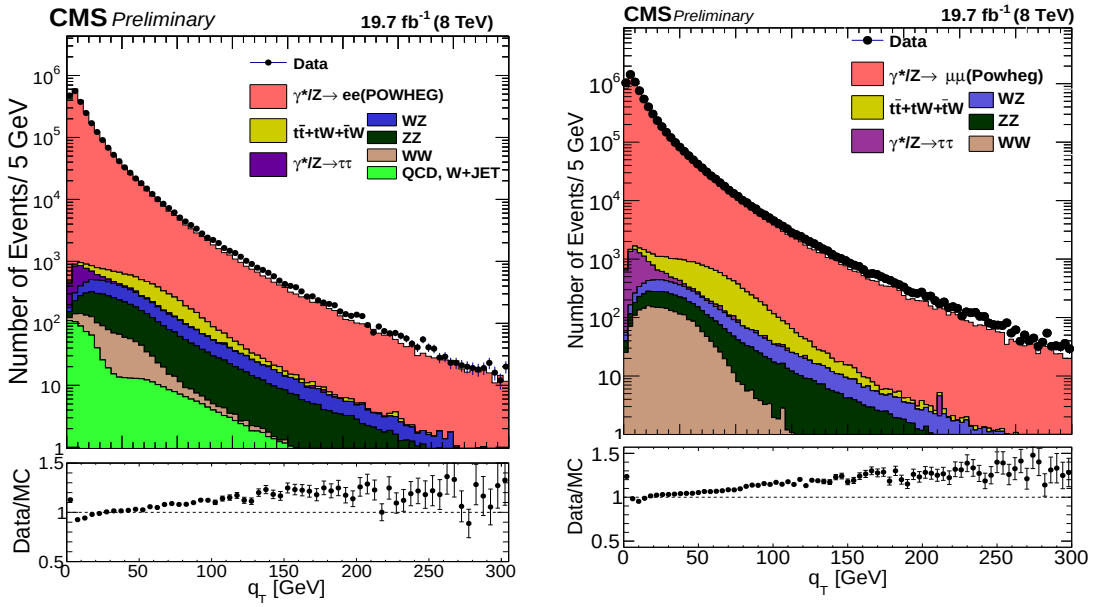

Figure 1: The spectrum of dilepton transverse momentum, before unfolding, in electron (left) and muon (right) channels overlaid with the distributions from POWHEG signal and background simulations normalized to luminosity. Only statistical uncertainties in data and simulation are indicated.

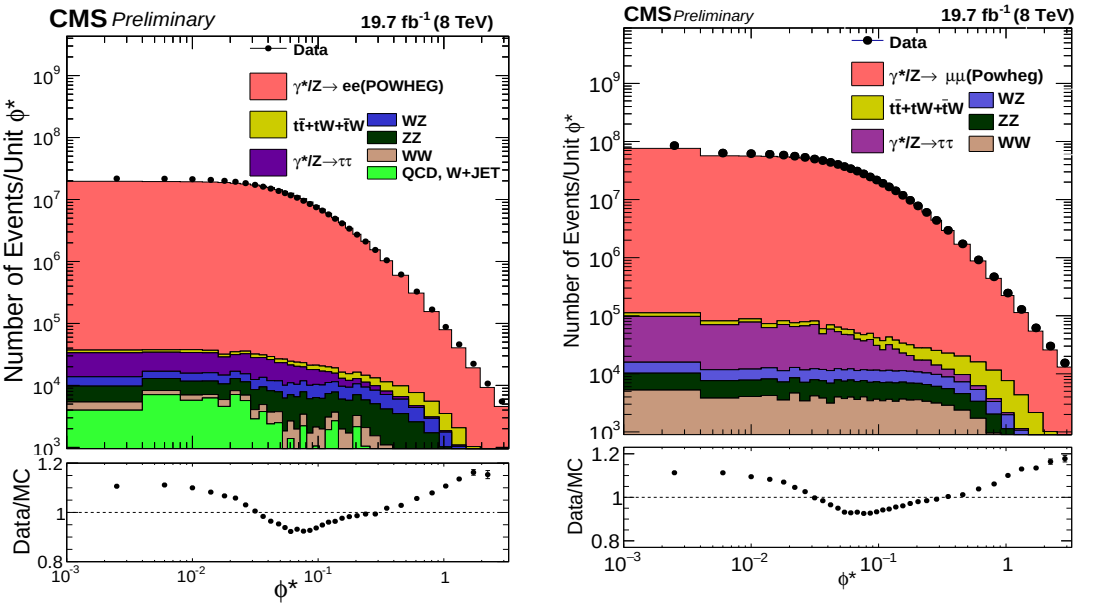

Figure 2: The ϕ^* distributions, before unfolding, in the dielectron (left) and dimuon (right) final states. POWHEG signal and background simulations, normalized to luminosity, are overlaid. Only statistical uncertainties in data and simulation are indicated.

4 Background Estimation

The background contributions to the selected event samples amount to only about 0.1% in both the electron and muon channels. The main component of this background consists of inclusive production of $t\bar{t}$, $Z \to \tau\tau$, WW, WZ, ZZ, single-top (tW and $W\bar{t}$), and, to a lesser extent, W + jets and QCD multijets. The latter two processes can contribute when a jet is misidentified as a lepton. Large simulated event samples have been used to estimate various background contributions. The MC prediction for the small background from top quark production has been validated at the level of 10% in [37] using CMS data.

The QCD multijets contribution in the muon channel is estimated with a muon-enriched sample of simulated QCD multijet events and is found to be negligible. The background from QCD multijet events in the electron channel is not negligible, however, because the probability for a jet to be misidentified as an elecrton is relatively higher. A data-driven method is used to estimate this background using a sample where the two electrons are required to have the same charge in addition to having passed all the selection requirements for the signal. This sample is dominated by Z events in which the charge of one of the electrons is mismeasured. Subsequently, for each bin of ϕ^* the invariant mass distribution of electron pairs is fitted with the combination of a Monte Carlo template and an analytic function based on a falling exponential multiplied by a complementary error function which terminates the exponential at low mass. The template is the sum of expected signal and background contributions($t\bar{t}$, $Z \to \tau\tau$, WW, WZ, ZZ, single-top (tW and $W\bar{t}$)) times a free parameter which allows for a different fraction of charge misidentification in data and simulation. The background due to QCD and W+jets in each ϕ^* bin for the electron channel is modeled by this analytic function. An uncertainty of 100% is assigned to this estimate. The QCD and W+jet background is estimated to be about 5% of the total background in the electron channel.

The estimated background is subtracted bin-by-bin before unfolding the spectra.

5 Unfolding the spectra

The differential cross section for the i-th bin of the ϕ^* spectrum, before unfolding, is

$$\left[\frac{\mathrm{d}\sigma}{\mathrm{d}\phi^*}\right]_i = \frac{\mathcal{N}_i - \mathcal{B}_i}{\mathcal{L}\,\Delta\phi_i^*}$$

where $\mathcal{N}_i$, $\mathcal{B}_i$ and $\Delta\phi_i^*$ are the number of events selected in data, the estimated number of background events and the width of the given bin, respectively. $\mathcal{L}$ is the total integrated luminosity. The acceptance and efficiency factors are incorporated into the values of $\mathcal{N}_i$ and $\mathcal{B}_i$.

Due to the finite resolution of the detector, measured values of ϕ^* are not exactly accurate, and the observed distribution may differ from the true one. In particular, events can migrate from one bin to the next; this migration amounts to 10% in the electron channel and 3% in the muon channel. Furthermore, final-state radiation (FSR) causes differences between the ideal spectrum and the observed one, even in the absence of measurement errors. To correct for these effects, the observed distributions are unfolded using the "iterative Bayesian" method [38], as implemented in the RooUnfold package [39]. The resolution model is taken from a large simulated signal sample generated with POWHEG interfaced to PYTHIA 6. The bias in unfolding due to the choice of generator, POWHEG vs. MADGRAPH, is not larger than 2%. The unfolded distributions, defined with respect to the fiducial kinematical region of the leptons, can be compared with theoretical predictions. The experimental identification of the lepton includes the photons from FSR lying within a certain cone radius. However the theoretical descriptions

of q_T used in this analysis are available in terms of leptons before FSR. Since FSR effects have been removed through unfolding, the unfolded distributions correspond to the Born level and the two channels can be combined directly.

6 Systematic Uncertainties

The total systematic uncertainty includes those due to luminosity, unfolding, Monte Carlo statistical uncertainties, pileup, background estimation, energy scale for electron channel, momentum scale and resolution for the muon channel, the efficiencies due to lepton selection (trigger, identification and isolation), the modeling of final state radiation (FSR) and the PDF uncertianties. The total uncertainty refers to the quadrature sum of the statistical and systematic components.

- The uncertainty on the measurement of the integrated luminosity, 2.6% [40], is uniform across the ϕ^* bins. This uncertainty vanished for the normalized differential cross section measurement.
- Choosing a particular event generator over another for unfolding a spectrum introduces a model dependence to the result. Replacing POWHEG by MADGRAPH results in relatively large statistical bin-to-bin fluctuations. By fitting a smooth analytical function to the ratio of the POWHEG and MADGRAPH results, the unfolding uncertainties can be assessed as a function of ϕ^*.
- The limited number of simulated signal events leads to statistical fluctations in the entries of the response matrix. The impact of these fluctuations is assessed using 500 pseudo-experiments in which the elements of the response matrix are varied within their statistical uncertainies.
- The uncertainties in the scale factors for the trigger, isolation and identification efficiencies were taken into account by varying the central value randomly using 500 pseudo-experiments to produce 500 sets of response matrices. The RMS of the distributions unfolded with these pseudo-experiments is taken as the uncertainty.
- To estimate the uncertainty from pileup, the cross section of the minimum bias events is varied by $\pm$ 5% . The maximum variation of the measured cross sections with respect to the nominal pileup scenario is taken as the systematic error. For the absolute cross section this uncertainty is approximately flat as a function of ϕ^* and amounts to about 0.4% for both electron and muon channels. For the normalised cross section the uncertainties remain well below 0.1% for most of the ϕ^* range but increase to above 0.2% in the highest ϕ^* bins for the electron channel.
- For $t\bar{t}$ background the assumed values of the cross sections are varied by 10% simultaneously to evaluate the systematic uncertainties in their contribution. In the electron channel the QCD and W+jet contribution is assigned a 100% uncertainty. For the absolute as well as the normalised cross sections in both channels the combined uncertainty is below 0.05% for ϕ^* below 0.15 but rises at higher ϕ^* to a maximum of 0.55% in the highest bin.
- The electron energy scale is known to a precision of 0.1 to 0.2%. The electron momentum thresholds were varied up and down by a conservative amount of 0.3% and the difference in the ϕ^* distribution after unfolding was taken as the systematic uncertainty. The uncertainty due to the resolution of electron energy is not considered separately. This uncertainty is approximately flat as a function of ϕ^* at around 0.15% for absolute cross section measurement and below 0.06% for the normalised

measurement.

- The muon momentum resolution is about 1.3 to 2% for the relevant p_T range. The muon momentum scale is corrected for the misalignments in the detector systems and the uncertainty in the magnetic field. To evaluate errors due to muon momentum scale mismeasurement the correction factors are varied using Gaussian random numbers within their uncertainties. The standard deviation in ϕ^* value resulting from these variations is assigned as a systematic uncertainty. This uncertainty is below 0.06% for the absolute and is below 0.04% for the normalised cross section measurement.
- To account for the uncertainty in QED FSR, the simulation is re-weighted to reflect the difference between a soft-collinear approach and the exact O(α) result. The difference between the measurements with and without re-weighting is assigned as an uncertainty. This uncertainty per bin is less than 0.08% for the absolute differential cross section measurement and less than 0.04% for the normalised cross section for both channels.
- The PDF uncertainty can affect the shape of the spectrum used to unfold the measurement in data. The POWHEG signal sample was produced using the CT10NLO PDF. The cross section uncertainty is assessed by generating the spectrum with each of the 52 eigenvectors of the CT10NLO sets and unfolding the data with each one. The differences in the unfolded spectrum with each of the up and the down eigenvectors taken separately with respect to the nominal PDF are added in quadrature to obtain the up and the down PDF uncertainties. The larger of the two is taken to be the PDF uncertianty in that bin. For the absolute cross section this uncertainty is approximately independent of ϕ^* around 0.2% (0.05%) for the electron (muon) channel, with a small decrease in the highest ϕ^* bins. For the normalised cross section this uncertainty is smaller than 0.05% for most of the ϕ^* range in both channels, with an increase in the highest ϕ^* bins to about 0.2% (0.1%) in the electron (muon) channel.

The variation of the total systematic uncertainty and its components for the absolute cross section measurement are presented in Fig. 3. The statistical uncertainty is also presented. The uncertainty due to unfolding includes the PDF uncertainty, the MC statistical uncertainty, and the dependence on the event generator. The uncertainties from the background estimation, pileup, and the electron energy scale or the muon p_T resolution are combined under the label *Other*. The total uncertainty for the absolute cross section measurement is dominated by the luminosity uncertainty, followed at low ϕ^* by the efficiency uncertainties and for $\phi^* > 1$ by the unfolding uncertainty.

The uncertainties for the normalized cross sections, shown in Fig. 4, are much lower than those for the absolute cross section due to the absence of a luminosity uncertainty. The variations due to different sources in electron and muon channels are somewhat different from those for the absolute cross section measurements, with the unfolding uncertainty generally dominating over the other uncertainties.

7 Results

The absolute differential cross sections $\mathrm{d}\sigma/\mathrm{d}\phi^*$ are presented in Fig. 5 (left) for the electron and muon channels. These cross sections are defined by the kinematic selection criteria for the leptons. The normalised differential cross sections $(1/\sigma)\,\mathrm{d}\sigma/\mathrm{d}\phi^*$ are shown in Fig. 5 (right). These measurements are compared to predictions from POWHEG. These predictions are normalised to

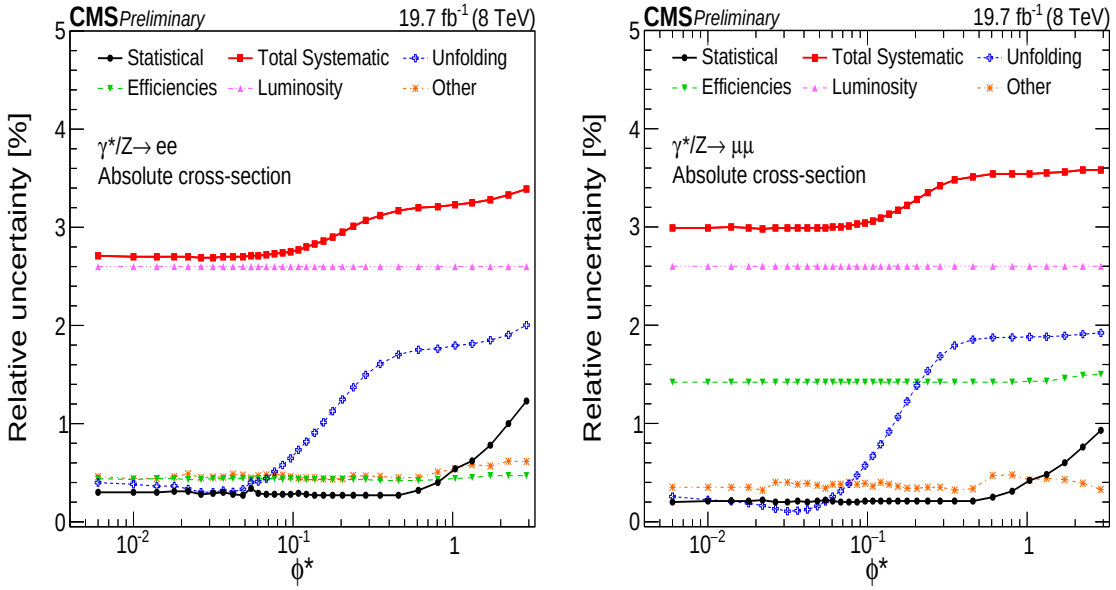

Figure 3: The variation of statistical and systematic uncertainties, for absolute cross section measurements, including the main components in electron (left) and muon (right) channels. The unfolding uncertainty includes those due to PDF, Monte Carlo statistics as well as possible bias in chosing a MC reference sample. The uncertainties from the background, pile-up and the electron energy scale or, the muon p_T resolution, as the case is, are combined under the label "Other".

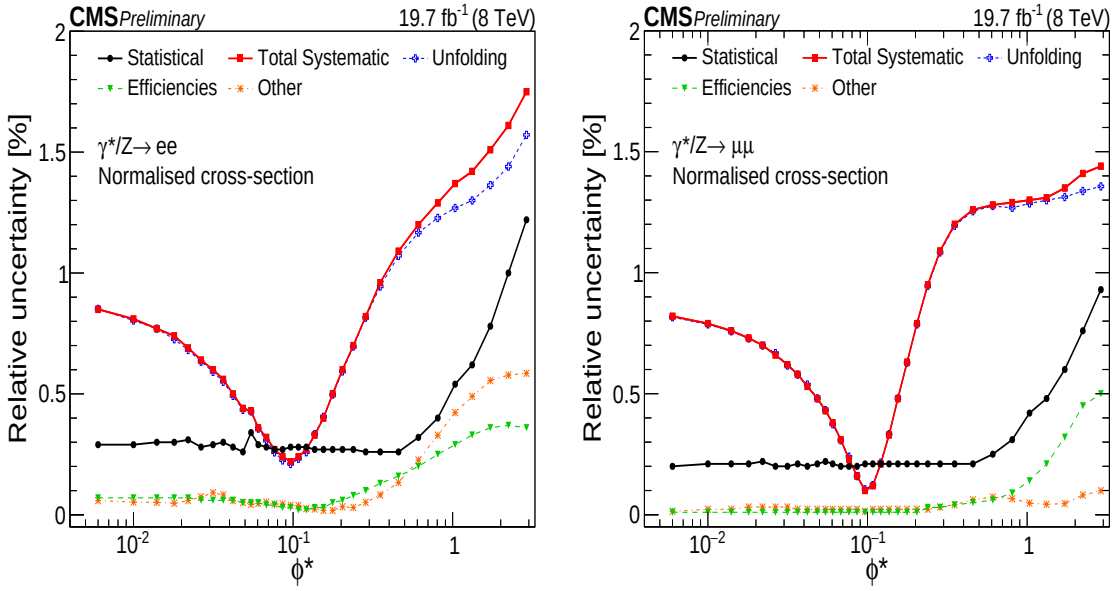

Figure 4: The variation of statistical and systematic uncertainties, for normalized cross section measurements, including the main components in electron (left) and muon (right) channels. The unfolding uncertainty includes those due to PDF, Monte Carlo statistics as well as possible bias in chosing a MC reference. The uncertainties from the background estimation, pile-up and the electron energy scale or, the muon p_T resolution, as the case is, are combined under the label "Other".

the NNLO value for the total cross section calculated using FEWZ. This normalisation includes an α_s uncertainty and a PDF uncertainty which together amount to 3.3%.

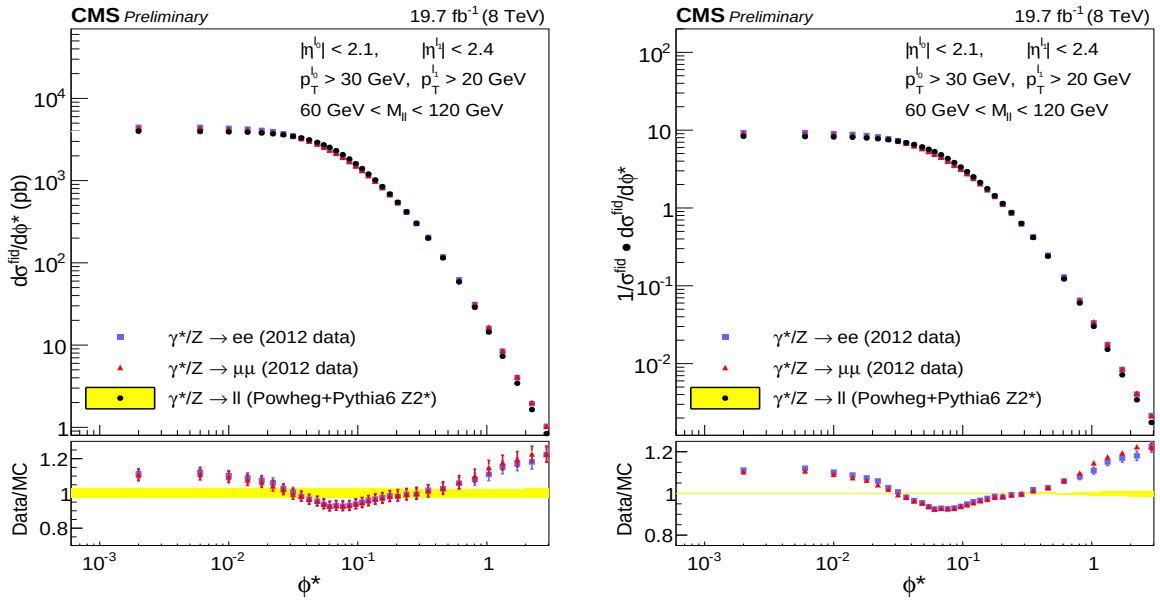

Figure 5: Absolute differential cross sections (left) and normalised differential cross sections(right) in the electron and muon channels. The horizontal band corresponds to the total uncertainty in the theoretical prediction from POWHEG: statistical, scale and PDF for the left plot and statistical and PDF for the right. The vertical bars correspond to the total uncertainty in the experimental measurements in electron and muon channels.

The differential cross section measurements in the electron and muon channels have been combined by computing a simple average of the corresponding central values. There are two components to the uncertainty. The uncorrelated uncertainties are added in quadrature. These include the uncertainty due to limited number of simulated events, the efficiency uncertainties, and the energy/momentum scale uncertainties. The fully correlated uncertainties due to luminosity, unfolding and background estimates, are added linearly. The pileup uncertainty, which is also correlated between the channels, is calculated by averaging the individual pileup distributions while the minimum bias cross section is varied by 5%. The maximum relative difference is taken as the error due to pileup. The three combined uncertainties (uncorrelated, correlated, and pileup) are added in quadrature to obtain the total uncertainty for the combined distribution.

The combined absolute and normalized differential cross sections are presented in Fig. 6. Predictions from three different theoretical calculations, including ResBos [41],MADGRAPH and POWHEG are also shown. The description by fixed-order perturbation theory diverges at lower limit of q_T, while the resummation techniques accounting for multiple gluon emissions from the incoming quarks lead to a tame behaviour in this region. The total cross section obtained from FEWZ has been used for the normalisation of the MADGRAPH and POWHEG predictions. The uncertainties shown for MADGRAPH indicate PDF and scale uncertainties in FEWZ. The uncertainty in ResBos is also due to PDF and scale uncertainties but is evaluated independently.

Figure 6 shows that none of the predictions match the measurements perfectly for the entire range of ϕ^*. While the maximum discrepancy of MADGRAPH and ResBos with respect to the data is below 5% (for the range $\phi^* < 0.1$), that of POWHEG is greater than 10%.

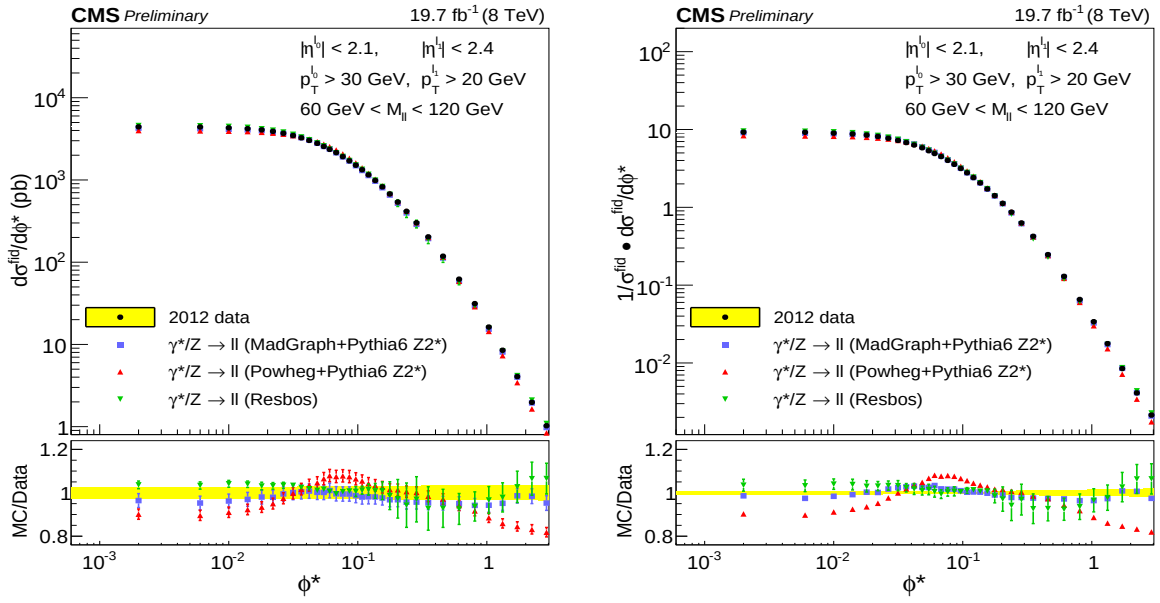

Figure 6: The combined absolute (left) and the normalized (right) cross sections compared to the predictions from POWHEG, MADGRAPH and ResBos. The horizontal band corresponds to the uncertainty in the experimental measurement. The vertical bars in the left plot correspond to the statistical, scale and PDF uncertainties in the theoretical predictions. In the right plot, the prediction from MADGRAPH has statistical uncertainty, POWHEG has statistical and PDF uncertainties and ResBos has statistical, scale and PDF uncertainties included.

The POWHEG event generator accounts for only one hard jet in the event. Consequently, the q_T spectrum is relatively soft leading to a smaller event yield and a significant disagreement in the high ϕ^* region. For this generator the uncertainty is dominated by the PDF uncertainty for the absolute and by the statistical uncertainty for the normalised distributions. The prediction from the MADGRAPH event generator, which produces inclusive DY events of Z production with up to 4 jets at leading order, matches with the data within about 3% over the whole range of ϕ^* considered in this analysis. The uncertainty in the prediction for the absolute distribution is dominated by the uncertainty on the total cross section computed with FEWZ and, for the normalised distribution, by the statistical uncertainty of the generated sample.

8 Conclusion

The kinematic variable ϕ^* is based on measurements of angles and is correlated with dilepton transverse momentum q_T in Drell-Yan events. A measurement of the absolute differential cross section $\mathrm{d}\sigma/\mathrm{d}\phi^*$ and the normalized differential cross section $(1/\sigma)\,\mathrm{d}\sigma/\mathrm{d}\phi^*$ has been presented based on 19.7 fb^{-1} of pp collision data recorded by the CMS detector. These measurements, conducted in both the electron and muon channels, provide a sensitive test for theoretical predictions. The absolute cross sections are defined with respect to the kinematic requirements set upon the leptons. The normalized cross sections, for which there is no uncertainty from the measurement of integrated luminosity, are precise at the level of 1 – 2%.

Comparisons to theoretical predictions have been made. In general the prediction from MADGRAPH shows better agreement with the data compared to the predictions from POWHEG and ResBos. Concerning the normalized differential cross sections, the differences with respect to

the measurements for $\phi^* < 0.1$ are at most 5% (ResBos), 4% (MADGRAPH) and 9% (POWHEG). For higher values of ϕ^* the differences are as high as 9%, 5% and 18% in the three cases respectively. In summary, none of the theoretical calculations succeed in predicting the measurements perfectly over the entire range of ϕ^*.

References

[1] C. Anastasiou, L. Dixon, and F. Petriello, "High precision QCD at hadron colliders: Electroweak gauge boson rapidity distributions at NNLO", *Phys. Rev. D* **69** (2004) 094008, doi:10.1103/PhysRevD.69.0S94008.

[2] K. Melnikov and F. Petriello, "Electroweak gauge boson production at hadron colliders through $O(\alpha_s^2)$", *Phys. Rev. D* **74** (2006) 114017, doi:10.1103/PhysRevD.74.114017.

[3] S. Alioli et al., "Drell-Yan production at NNLL+NNLO matched to parton showers", *Phys. Rev.* **D92** (2015), no. 9, 094020, doi:10.1103/PhysRevD.92.094020, arXiv:1508.01475.

[4] CMS Collaboration, "Measurement of the differential and double-differential Drell-Yan cross sections in proton-proton collisions at $\sqrt{s} = 7$ TeV", *JHEP* **12** (2013) 030, doi:10.1007/JHEP12(2013)030, arXiv:1310.7291.

[5] CMS Collaboration, "Measurements of differential and double-differential Drell-Yan cross sections in proton-proton collisions at $\sqrt{s}$ = 8 TeV", *Eur. Phys. J. C* **75** (Dec, 2014) 147. 39 p. Comments: Submitted to Eur. Phys. J. C.

[6] ATLAS Collaboration, "Measurement of the low-mass Drell-Yan differential cross section at $\sqrt{s}$ = 7 TeV using the ATLAS detector", *JHEP* **06** (2014) 112, doi:10.1007/JHEP06(2014)112, arXiv:1404.1212.

[7] ATLAS Collaboration, "Measurement of the high-mass Drell–Yan differential cross-section in pp collisions at sqrt(s)=7 TeV with the ATLAS detector", *Phys. Lett.* **B725** (2013) 223–242, doi:10.1016/j.physletb.2013.07.049, arXiv:1305.4192.

[8] Y. Li and F. Petriello, "Combining QCD and electroweak corrections to dilepton production in FEWZ", *Phys.Rev.* **D86** (2012) 094034, doi:10.1103/PhysRevD.86.094034, arXiv:1208.5967.

[9] ATLAS Collaboration, "Measurement of the transverse momentum distribution of Z/gamma* bosons in proton-proton collisions at $\sqrt{s} = 7$ TeV with the ATLAS detector", *Phys.Lett.* **B705** (2011) 415–434, doi:10.1016/j.physletb.2011.10.018, arXiv:1107.2381.

[10] LHCb Collaboration, "Measurement of the cross-section for $Z \to e^+e^-$ production in pp collisions at $\sqrt{s} = 7$ TeV", *JHEP* **1302** (2013) 106, doi:10.1007/JHEP02(2013)106, arXiv:1212.4620.

[11] CMS Collaboration, "Measurement of the Rapidity and Transverse Momentum Distributions of Z Bosons in pp Collisions at $\sqrt{(s)}$=7 TeV", *Phys.Rev.* **D85** (2012) 032002, doi:10.1103/PhysRevD.85.032002, arXiv:1110.4973.

[12] CMS Collaboration, "Measurement of the transverse momentum distributions of Z Bosons decaying to dimuons in pp collisions at $\sqrt{s}$ =8 TeV", Technical Report CMS-PAS-SMP-12-025, CERN, Geneva, 2013.

[13] S. Hoeche, Y. Li, and S. Prestel, "Drell-Yan lepton pair production at NNLO QCD with parton showers", *Phys. Rev.* **D91** (2015), no. 7, 074015, doi:10.1103/PhysRevD.91.074015, arXiv:1405.3607.

[14] CMS Collaboration, "Measurement of the Z boson differential cross section in transverse momentum and rapidity in protonproton collisions at 8 TeV", *Phys. Lett.* **B749** (2015) 187–209, doi:10.1016/j.physletb.2015.07.065, arXiv:1504.03511.

[15] A. Banfi et al., "Optimisation of variables for studying dilepton transverse momentum distributions at hadron colliders", *Eur.Phys.J.* **C71** (2011) 1600, doi:10.1140/epjc/s10052-011-1600-y, arXiv:1009.1580.

[16] A. Banfi, M. Dasgupta, S. Marzani, and L. Tomlinson, "Predictions for Drell-Yan ϕ^* and Q_T observables at the LHC", *Phys.Lett.* **B715** (2012) 152–156, doi:10.1016/j.physletb.2012.07.035, arXiv:1205.4760.

[17] S. Marzani, "Q_T and ϕ^* observables in Drell-Yan processes", *EPJ Web Conf.* **49** (2013) 14007, doi:10.1051/epjconf/20134914007.

[18] D0 Collaboration, "Precise study of the Z/γ^* boson transverse momentum distribution in $p\bar{p}$ collisions using a novel technique", *Phys. Rev. Lett.* **106** (2011) 122001, doi:10.1103/PhysRevLett.106.122001, arXiv:1010.0262.

[19] ATLAS Collaboration, "Measurement of angular correlations in Drell-Yan lepton pairs to probe Z/gamma* boson transverse momentum at $\sqrt{s}$ =7 TeV with the ATLAS detector", *Phys. Lett.* **B720** (2013) 32–51, doi:10.1016/j.physletb.2013.01.054, arXiv:1211.6899.

[20] CMS Collaboration, "Particle-flow event reconstruction in CMS and performance for jets, taus, and MET", *CMS-PAS-PFT-09-001* (2009).

[21] CMS Collaboration Collaboration, "Commissioning of the Particle-flow Event Reconstruction with the first LHC collisions recorded in the CMS detector", Technical Report CMS-PAS-PFT-10-001, 2010.

[22] CMS Collaboration, "Electron reconstruction and identification at $\sqrt{s}$ = 7 TeV", Technical Report CMS-PAS-EGM-10-004, CERN, Geneva, 2010.

[23] CMS Collaboration, "Performance of CMS muon reconstruction in pp collision events at $\sqrt{s} = 7$ TeV", *JINST* **7** (2012) P10002, doi:10.1088/1748-0221/7/10/P10002, arXiv:1206.4071.

[24] CMS Collaboration, "Measurement of the Inclusive W and Z Production Cross Sections in pp Collisions at $\sqrt{s} = 7$ TeV", *JHEP* **10** (2011) 132, doi:10.1007/JHEP10(2011)132, arXiv:1107.4789.

[25] P. Nason, "A new method for combining NLO QCD with shower Monte Carlo algorithms", *JHEP* **11** (2004) 040, doi:10.1088/1126-6708/2004/11/040, arXiv:hep-ph/0409146.

[26] S. Alioli, P. Nason, C. Oleari, and E. Re, "A general framework for implementing NLO calculations in shower Monte Carlo programs: the POWHEG BOX", *JHEP* **1006** (2010) 043, doi:10.1007/JHEP06(2010)043, arXiv:1002.2581.

[27] S. Alioli, P. Nason, C. Oleari, and E. Re, "Vector boson plus one jet production in POWHEG", *JHEP* **01** (2011) 095, doi:10.1007/JHEP01(2011)095, arXiv:1009.5594.

[28] S. Frixione, P. Nason, and C. Oleari, "Matching NLO QCD computations with Parton Shower simulations: the POWHEG method", *JHEP* **11** (2007) 070, doi:10.1088/1126-6708/2007/11/070, arXiv:0709.2092.

[29] J. Gao et al., "CT10 next-to-next-to-leading order global analysis of QCD", *Phys.Rev.* **D89** (2014), no. 3, 033009, doi:10.1103/PhysRevD.89.033009, arXiv:1302.6246.

[30] T. Sjostrand, S. Mrenna, and P. Z. Skands, "PYTHIA 6.4 Physics and Manual", *JHEP* **05** (2006) 026, arXiv:hep-ph/0603175.

[31] R. Field, "Early LHC Underlying Event Data - Findings and Surprises", (2010). arXiv:1010.3558.

[32] CMS Collaboration, "Measurement of the Underlying Event Activity at the LHC with $\sqrt{s} = 7$ TeV and Comparison with $\sqrt{s} = 0.9$ TeV", *JHEP* **1109** (2011) 109, doi:10.1007/JHEP09(2011)109, arXiv:1107.0330.

[33] J. Alwall et al., "MadGraph 5 : Going Beyond", *JHEP* **1106** (2011) 128, doi:10.1007/JHEP06(2011)128, arXiv:1106.0522.

[34] P. Nadolsky et al., "Progress in CTEQ-TEA PDF Analysis", doi:10.3204/DESY-PROC-2012-02/301, arXiv:1206.3321.

[35] M. Czakon and A. Mitov, "Top++: A Program for the Calculation of the Top-Pair Cross-Section at Hadron Colliders", *Comput.Phys.Commun.* **185** (2014) 2930, doi:10.1016/j.cpc.2014.06.021, arXiv:1112.5675.

[36] GEANT4 Collaboration, "GEANT4: A simulation toolkit", *Nucl. Instrum. Meth.* **A506** (2003) 250–303, doi:10.1016/S0168-9002(03)01368-8.

[37] CMS Collaboration, "Comparison of the Z/γ + jets to γ + jets cross sections in pp collisions at $\sqrt{s} = 8$ TeV", *JHEP* **10** (2015) 128, doi:10.1007/JHEP04(2016)010, 10.1007/JHEP10(2015)128, arXiv:1505.06520. [Erratum: JHEP04,010(2016)].

[38] G. D'Agostini, "A multidimensional unfolding method based on Bayes' theorem", *Nuclear Instruments and Methods in Physics Research A* **362** (February, 1995) 487–498, doi:10.1016/0168-9002(95)00274-X.

[39] H. B. Prosper and L. Lyons, "Proceedings, PHYSTAT 2011 Workshop on Statistical Issues Related to Discovery Claims in Search Experiments and Unfolding, CERN,Geneva, Switzerland 17-20 January 2011", doi:10.5170/CERN-2011-006.

[40] CMS Collaboration, "CMS Luminosity Based on Pixel Cluster Counting - Summer 2013 Update", Technical Report CMS PAS LUM-13-001, CERN, Geneva, 2013.

[41] G. Ladinsky and C. Yuan, "The Nonperturbative regime in QCD resummation for gauge boson production at hadron colliders", *Phys.Rev.* **D50** (1994) 4239, doi:10.1103/PhysRevD.50.R4239, arXiv:hep-ph/9311341.